Acta of Bioengineering and Biomechanics
Vol. 24, No. 4, 2022

Original paper
DOI: 10.37190/ABB-02157-2022-02

Differential evolution and cost-maps for needle path planning in Baker's cyst aspiration

ADAM CISZKIEWICZ[1]*, JACEK LORKOWSKI[2], GRZEGORZ MILEWSKI[3]

[1] Faculty of Mechanical Engineering, Cracow University of Technology, Kraków, Poland.
[2] Department of Orthopaedics, Traumatology and Sports Medicine,
Central Clinical Hospital of the Ministry of the Interior and Administration in Warsaw, Warsaw, Poland.
[3] Faculty of Mechanical Engineering, Cracow University of Technology, Kraków, Poland.

Purpose: The Baker's cysts appear within the popliteal fossa along with the progression of degenerative changes. Removal of its contents through aspiration is often a necessary complement to treatment at various stages of the development of gonarthritis. *Methods*: The paper presented a procedure for needle automatic needle path planning in cyst aspiration in transverse plane. The method was based on optimization and used a custom objective function, which utilized cost maps obtained from preprocessed, segmented images of the knee. The optimization was carried out with Differential Evolution. Furthermore, a preliminary sensitivity analysis was carried out. The obtained paths were compared to the reference paths proposed by an experienced surgeon. *Results*: The procedure was tested on 165 numerical simulations. In all of the obtained paths, the needle successfully avoided crucial objects, such as veins, arteries and nerves. Furthermore, the overall travel distance in the joint was also minimized. When compared to the reference from the surgeon, 90% of the paths were almost the same or only slightly different. Furthermore, the remaining 10% of the generated paths were viable but different. *Conclusion*: Based on the obtained results, the proposed solution could be a viable solution for planning the aspiration of Baker's cyst.

Key words: *image analysis, computer simulation, needle insertion*

1. Introduction

Osteoarthritis was for many years the most common joint disease in adults worldwide. Its incidence rises with age. Clinically significant changes from the epidemiological point of view most often concern the spine, hip and knee joints [26]. The ongoing and increasing epidemic of arthritis for several decades was one of the reasons why the WHO organized "Decade of the Bones and Joints: 2000–2010". Standard methods of gonarthritis treatment are: pharmacotherapy, rehabilitation treatment, supplementation of hyaluronic acid derivatives, orthobiologics, arthroscopic procedures, osteotomies, unicompartment and total knee arthroplasty [4], [8], [14], [19].

The so-called Baker's cysts appear within the popliteal fossa along with the progression of degenerative changes [1]. Removal of Baker's cyst or its contents is often a necessary complement to treatment at various stages of the development of gonarthritis. The need to remove the cyst most often results from the limitation of the range of motion in the knee joint and the symptoms of compression on the structures of the popliteal fossa [36], [40]. The range of motion could be further reduced by osteoarthritis and coxarthritis [13], [37]. Baker's cysts are most often located in the posteromedial region of the knee between the medial belly of the gastrocnemius muscle and semimembranosus tendon [12]. The Baker's cyst forms through a connection between the knee joint and a bursa [12]. It has been known for many years that the most

* Corresponding author: Adam Ciszkiewicz, Faculty of Mechanical Engineering, Cracow University of Technology, Cracow, Poland. E-mail: adam.ciszkiewicz@pk.edu.pl
Received: November 23rd, 2022
Accepted for publication: January 26th, 2023

frequently associated pathologies are meniscal lesions (lesions of the medial meniscus in 82% of the cases and of lesions of the lateral meniscus in 38%) and degenerative changes of the articular cartilage [18].

Differential diagnostics include an interview, physical examination and radiological diagnostics. It is imperative to pay attention to Foucher's sign during the physical examination. The Baker's cyst decreases with 45 degrees of knee joint flexion [7]. Ultrasound examination and MRI are useful in radiological diagnostics. Ultrasonography allows us to evaluate fluid the tumor content and cyst location [6], [31]. An accurate and comparable study can be done by MRI [16], [31]. Effective treatment should be causal and include treatment of the osteoarthritis. The aspiration and possible, additionally, local injection of corticosteroids is an emergency action, decompressing the compression symptoms within the popliteal fossa as it presents a high rate of recurrence of the cyst [15], [27]. So it only makes sense as a temporary measure and is not a complete, proper treatment. However, such action is needed in the case of pressure symptoms or as an adjunct to causal treatment.

In recent years, a paradigm shift can be observed in robotics and specifically in computer aided surgery, as seen in the growing number of research papers in this field [22], [28]. This interest can be explained by the increasing shortages in the health sector combined with the ageing of the world population. The focus is now put on autonomous and semi-autonomous surgery as it can potentially offload surgeons. The current research is mostly focused on: presurgery planning [3], [25], guided surgery [32], [34] and tele-surgery [29]. A crucial aspect of planning for autonomous or semi-autonomous surgical procedures is the path planning for medical instruments. While there are many methods available for path planning in 2D and 3D space for robotic applications [2], [10], [30], [33], the problem is still complex when considering surgical procedures. Such techniques have been employed in endovascular surgery [17], surgeon training systems [30] and steerable needle insertion [38]. Nevertheless, to the best of our knowledge these approaches have not been applied in modeling knee joint surgery, or specifically for needle path planning in cyst aspiration.

The aim of this study was to develop a method for optimal needle path planning in Baker's cyst aspiration in the transverse plane. Based on the segmented image of the knee, the procedure estimated the target aspiration point, preprocessed the images and computed the cost map. Then, the optimal needle aspiration path in the transverse plane, which included aspiration point and angle, was obtained using numerical optimization with Differential Evolution (DE). The results were then critically compared to the reference paths proposed by an experienced surgeon.

2. Method

Based on the segmented two-dimensional input image of the knee joint in the transverse plane. First, a cost map for path optimization and an estimate for the target point were obtained. After that, the optimal needle aspiration point and angle in the transverse plane were obtained using DE. The most important aspects of the procedure were explained in the following paragraphs.

2.1. The input data set

The input to the proposed procedure was a segmented image of the knee in the transverse plane. This was in line with medical practice, as cyst aspiration is often carried out in the transverse plane or a plane close to it. In the images, each region of the knee had a separate color (Fig. 1a). Along with these images, a weight matrix was supplied. The weight matrix contained the weights of the regions, i.e., numerical values representing the cost of traversing the knee regions (the higher the number, the more costly/dangerous the region was).

The segmented image contained separate regions for:

- bones,
- muscle tissue,
- fat tissue along with skin,
- nerves,
- veins and arteries,
- cyst,
- operational space.

The weights for each region were consulted with a clinician (the second author) based on medical practice. The veins, arteries and nerves were assigned the maximal value of 100.0, while the operational space was set to 0.0. The muscle tissue and the fat were considered fairly safe to transverse with weights set to 20.0 and 1.0, respectively. The bones had their weight set at 2.0 – in practice, the search was constrained to the posterior part of the knee and the possibility of reaching the bones was limited. Also, higher weight for the bones caused numerical problems in some cases. The cyst's weight was set to 0.0, because the cost of traversing the cyst was directly included in

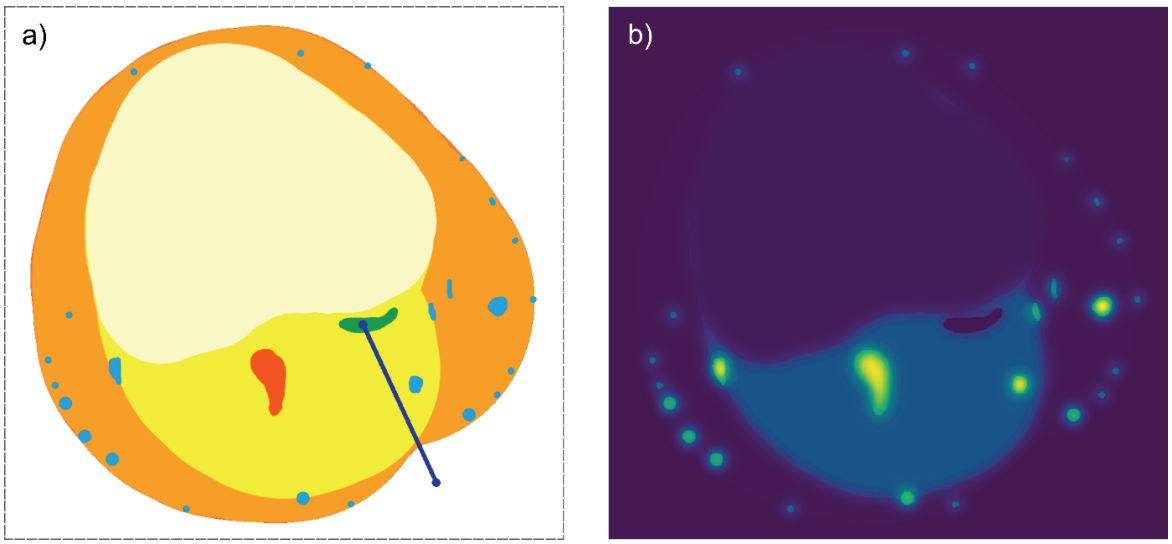

Fig. 1. a) A sample segmented knee image along with the needle path provided by the surgeon, b) a cost map generated from the image using the proposed method (brighter colors signify regions more costly to traverse)

the objective function, described in the following sections.

In this study, the images were manually segmented by an experienced clinician. Each region of the knee was assigned a different, unique color. Furthermore, each image also contained a needle path proposed the surgeon based on clinical practice. This path can be used as a reference when assessing the results obtained from the procedure.

2.2. Obtaining the cost map

In typical path planning problems the domain is usually partitioned into two sets: the collision-free and the collisive set. A path, which contains collisions is often considered unfeasible. Therefore, the main aim for the search procedure is to find a path, which does not contain any collisions (and then potentially optimize it). The approach used in this study was based on slightly different assumptions. The domain was treated as one set, in which every point was accessible but also had a traversion-cost assigned to it. This meant that, even theoretically, there could not be a collision-free path, however, the paths could still be compared – the one with the lower cost of traversability was considered better. This soft approach to path planning is less common in mobile robotics but it can be useful in medical problems. In order to perform to such an optimization, a cost map, which contains the traversion-cost for every point, was needed. The process of obtaining it was described below.

As mentioned before, the input data set to the procedure consisted of segmented images of seven regions in the knee. These images represented the Baker's cyst as well as other regions of the knee with different weights. The preconditioning of the images was performed in three steps. Firstly, the color image was transformed into monochrome, in which pixels of different regions had their value based on the previously-mentioned region weights (Section 2.1). This step return a preliminary cost map for path planning. In order to add customizability to this model as well increase the safety of the procedure, the obtained map was additionally blurred with Gaussian filtering. The obtained blurred image was then added with a weighted sum to the original map, creating a final customizable representation of the collision space. This procedure resulted in a basin-like collision-space, in which even the vicinity of important and delicate elements was costly to traverse. It is worth emphasizing that the parameters used for obtained could be customized. In the latter part of the study, the sensitivity of the procedure to these elements was also analyzed. The process of obtaining the final cost map was summarized in Eq. (1):

$$cost\_map_{fin} = cost\_map_{ini} + s[gaussian\_filter(cost\_map_{ini}, \sigma)], \quad (1)$$

where: $cost\_map_{fin}$ – the final cost map representing the collision space, $cost\_map_{ini}$ – the initial cost map, s – the scale factor, which determines how blurred the final image was, $gaussian\_filter()$ – the Gaussian filter (blur) function, which depends on one parameter, the standard deviation σ.

A sample image presenting a final cost map obtained with the proposed method was presented in Fig. 1b.

2.3. The vector of decision variables

The vector of decision variables $\boldsymbol{x}$ represented the two-dimensional path for the needle in the transverse plane and was written as follows:

$$\boldsymbol{x} = [x_{target} \quad y_{target} \quad \theta]^T, \tag{2}$$

where: x_{target} (y_{target}) – the x (y) coordinate of the target point for the aspiration in the transverse plane; θ – the approach angle for the needle in the transverse plane.

It contained three components, two of which were the coordinates of the target point for the aspiration. The third element of $\boldsymbol{x}$ represented the angle of approach for the needle. In total, the path of the needle aspiration in the transverse plane was simplified into three variables. Some additional constraints were put on the target point. Namely, within the objective function it was bound to be relatively close to the center of the largest empty circle (LEC) inside the cyst based on [9].

2.4. The objective function

In this study, the objective function was composed of two separate criteria and computed using a weighted average.

The first criterion signified the number of weighted collisions between the needle and the knee. Computing the collisions with the previously obtained collision map was a multi-stage process. Firstly, a binary image of the needle swiped through its path was obtained. The image was of the same resolution as the collision map. The needle was simplified into a rectangular shape, which was oriented and located based on the vector of decision variables, while taking into account the size of the collision map and its edges. The value of 1 was assigned to pixels representing the needle, while the background was set to 0. Then, a multiplication operation was performed between the obtained needle image and the final cost map. This resulted in an image, where only the parts covered by the needle had values higher than 0. In order to compute the traversion-cost for needle, a simple sum operation was performed on the final image. This value, the collision sum – *collision_sum*, constituted the first part of the objective function:

$$f(\boldsymbol{x}) = w_1 \cdot collision\_sum + w_2 \cdot dist, \tag{3}$$

where: *collision_sum* – the sum of collisions between the needle and the final cost map, *dist* – the second criterion based on a nonlinearly scaled distance between the target point and the LEC center, w_1/w_2 – the weights of the subobjectives.

The first criterion – *collision_sum* – took the travel distance and cost for the needle into account. Nevertheless, it was also necessary to explicitly include the aspiration point in the objective, to make sure that the algorithm took its location into account, while minimizing the traversion-cost. This was done using a second criterion – *dist* (Eq. (3)), which was formulated as a nonlinear distance between the target point and the center of the LEC inside the cyst, which was computed using the method presented in [9]. Our initial simulations suggested that simply adding the Euclidean distance as the second criterion was not enough to ensure that the target would be inside the cyst. Therefore, nonlinear scaling was used on the distance. For distances smaller than 70% of the radius of the LEC r_{LEC}, the distance scaled linearly. Nevertheless, if the distance exceeded 70% of r_{LEC}, it was squared and multiplied by 5. This returned a much higher value and in practice worked similarly to a penalty function, which ensured that the target would not be outside the cyst. The actual value of the criterion was calculated based on the following formula:

$$dist = \begin{cases} if\ dist_{target-LECcenter} < 0.7 \cdot r_{LEC}, & then: dist_{target-LECcenter} \\ if\ dist_{target-LECcenter} < 0.7 \cdot r_{LEC} & then: 5 \cdot dist^2_{target-LECcenter} \end{cases} \tag{4}$$

where: *dist* – the value of the second criterion in the objective function, $dist_{target\text{-}LECcenter}$ – the Euclidean distance between the target point and the center of the LEC inside the cyst, r_{LEC} – the radius of the LEC inside the cyst.

As mentioned before, the two subobjectives – *collision_sum* and *dist* – described in the previous paragraphs formed the final objective function with weighted sum as can be seen in Eq. (3).

2.5. The optimization procedure

The optimization routine used in this paper is DE [35]. DE is a modern representative of a large group of metaheuristic optimization algorithms referred to as evolutionary computation, which also include different algorithms used in varied applications [2], [10], [11], [23]. In DE, the optimization proceeds by iterating over a set of solutions and is gradually improved using differential operators, which mix and mutate the solutions. Its main advantages over other optimization methods are: global search and no need for differentiable objective function.

2.6. The sensitivity analysis

In order to verify the behavior of the proposed procedure a preliminary sensitivity analysis was carried out. The path planning procedure was repeated 15 times for each of the studied 11 cases. The first variant (*id* = 1, Table 1) was finetuned manually, so that the returned paths would be clinically viable and it served as a basis for other variants. In every iteration, one of the parameters of the procedure was modified to check the sensitivity of the method to that parameter.

The parameters included the weights of the collisive regions, the scaling and blur factor for preprocessing the images, the weights of the objective function and selected aspects of DE, namely: population size and number of generations. After each run, the script logged the values of the objective function for the generated path and the path proposed by the surgeon as well as a visual representation of the paths on the cost map.

The weights for the operational tissue and fat were set at 0 and 1 respectively and due to their lower significance the surgical procedure – they were not included in the analysis. As the cyst was already included in the second subobjective of the objective function, its weight was also set to 0 and not modified during the test.

In order to numerically compare the paths proposed by the surgeon to the ones generated by the procedure, the following relative indicator was computed for each case within each procedure variant (3):

$$rel\_diff = [(f(x_s) - f(x_g))/f(x_g)] \cdot 100\%, \quad (5)$$

where: *rel_diff* – the indicator of the relative difference between the path from the surgeon and the generated one; this indicator was computer for each case within each variant of the procedure (in total: 165 times), $f(x_s)/f(x_g)$ – the value of the objective function for the path, which was proposed by the surgeon/generated by the procedure.

3. Results

The proposed method was tested using 11 segmented images of the knee over 15 different variants of the procedure. All of the 165 of the paths generated by the procedure were safe and viable. When compared to the reference paths proposed by the surgeon, three different trends were observed. Namely, the path obtained with the procedure could be:

- almost the same as the reference path (45% of the results),
- slightly different from the path proposed by the surgeon (45% of the results),
- significantly different from the path proposed by the surgeon (10%).

In almost half of the studied cases, the difference between the path proposed by the surgeon and the computer-generated one was negligible or the paths were highly similar. An example of such a case was presented in Fig. 2. Both paths were safe – all of the important structures were avoided with safe distance,

Table 1. The variants of the procedure tested during the preliminary analysis of sensitivity, where: *id* – the id number of the procedure variant, *max_gen* – number of generations in DE, *pop_size* – number of solutions in each generation, w_1 and w_2 – the weights of the subobjectives in the objective function, s and σ – the parameters used to obtain the final cost map (Section 2.2), $w_b/w_m/w_n/w_{v,a}$ – the weight for the bone/muscle/nerves/veins and arteries used for computing the final cost map (Sections 2.1 and 2.2)

id	*max_gen*	*pop_size*	w_1	w_2	*scale*	*sigma*	w_b	w_m	w_n	$w_{v,a}$
1	60	180	1	15	6	11	2	20	100	70
2	30	180	1	15	6	11	2	20	100	70
3	90	180	1	15	6	11	2	20	100	70
4	60	90	1	15	6	11	2	20	100	70
5	60	270	1	15	6	11	2	20	100	70
6	60	180	5	15	6	11	2	20	100	70
7	60	180	10	15	6	11	2	20	100	70
8	60	180	1	15	3	11	2	20	100	70
9	60	180	1	15	9	11	2	20	100	70
10	60	180	1	15	6	6	2	20	100	70
11	60	180	1	15	6	16	2	20	100	70
12	60	180	1	15	6	11	2	60	100	70
13	60	180	1	15	6	11	42	20	100	70
14	60	180	1	15	6	11	2	20	60	70
15	60	180	1	15	6	11	2	20	100	30

while the overall travel distance was also minimized. The target points in both approaches were close to the center of the largest empty circle for the cyst or its widest cross-section. Furthermore, both paths would be easy to execute in an actual clinical scenario.

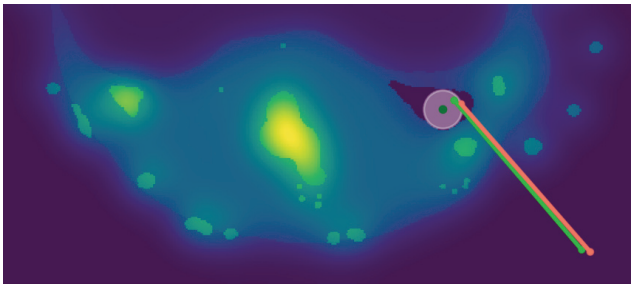

Fig. 2. An example of a generated path (green color) that was almost the same as the path proposed by the surgeon (red color)

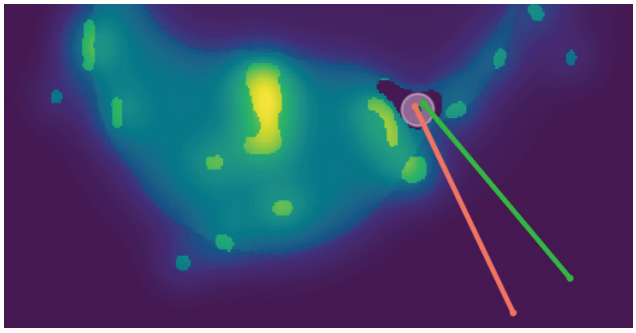

Fig. 3. An example of a generated path (green color) that was slightly different from the path proposed by the surgeon (red color)

In Figure 3, a trend is shown, in which the paths of the surgeon differed from the generated ones, but only very slightly. It can be seen that the paths were conceptually similar, the only observable difference was in travel distance over muscle tissue. In this case, the path obtained from the procedure was less invasive – or, in other words, shorter within the knee joint.

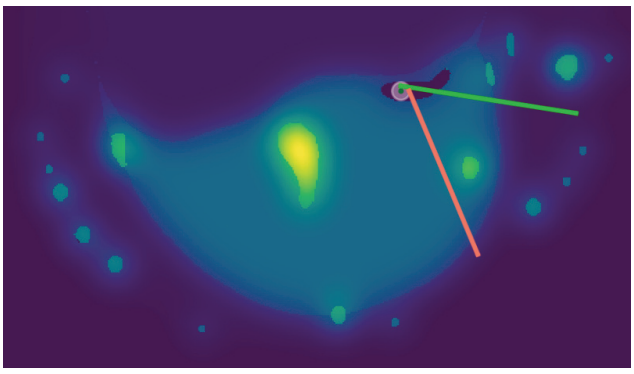

Fig. 4. An example of a generated path (green color) that was significantly different from the path proposed by the surgeon (red color)

An example of a case in which the path obtained with the procedure differed significantly from the one proposed by the surgeon was presented in Fig. 4.

A summary of the obtained results was presented in Table 2. In general, in all of the studied cases the value of the objective function was lower for the generated path when compared to the path given by the surgeon. This suggested that the computed paths were more optimal in terms of the assumed objective – 80% better on average.

Table 2. A summary of the results obtained from each variant of the procedure, when the generated paths were compared to the reference provided by the surgeon with the relative difference indicator (Eq (3) in Section 2.4), where min, max, avg indexes stand for minimal, maximal and average values

id	rel_diff_{min} [%]	rel_diff_{max} [%]	rel_diff_{avg} [%]
1	27.13	99.77	80.31
2	26.81	99.77	80.10
3	27.47	99.77	80.31
4	27.72	99.77	80.20
5	27.72	99.77	80.35
6	24.93	99.81	79.33
7	25.14	99.82	79.87
8	28.51	99.87	81.62
9	27.64	99.77	79.70
10	23.20	99.90	83.31
11	24.80	99.72	78.23
12	18.95	99.89	79.07
13	27.41	99.77	81.06
14	23.38	99.79	79.77
15	27.95	99.77	80.08

4. Discussion

Based on the obtained results, it could be concluded that the first and the second trend validated the proposed procedure. Nevertheless, in terms of novelty, the most interesting cases were found in the third trend, in which the approach proposed by the surgeon differed significantly from the path that was generated. Within this trend, the generated paths minimized the travel among all of the soft tissues – this included the fat tissue and the muscle tissue as well. On the other hand, the paths proposed by the surgeon were mostly focused on avoiding the arteries and nerves based on the premise that muscle and fat tissue damage can be neglected. However, it should be mentioned, that in both of these approaches, the needle did not penetrate the arteries and nerves. The paths proposed by the surgeon also took into account the practical aspects of positioning the patient during surgery.

The proposed angles of approach would be easier to execute with the available medical equipment. Nevertheless, the generated paths could be seen as interesting and potentially viable. However, additional constraints regarding the operational space should be included in the optimization.

In terms of the objective function, the raw numerical values suggested that the paths obtained with the proposed procedure were more optimal than the reference, it would be difficult to ascertain whether the assumed objective contained all of the aspects important in surgical procedures. Therefore, these results should be interpreted with caution.

On the other hand, it could be seen that the parameters of the procedure had a significant effect on the output. This suggested that a further study with a more complete sensitivity analysis should be carried out. Based on the current results, it can be seen that the variant 11 returned the closest results to the reference provided by the surgeon. In this case, the value of the standard deviation for the Gaussian blur was increased and the resulting cost map had softer transitions between regions. On the other hand, the biggest difference between the paths proposed by the surgeon and the generated ones was obtained with the variant 10, in which the standard deviation was decreased. This showed that the image preprocessing phase highly impacted the results. The problem should be studied more within a comprehensive sensitivity analysis. Potentially, by tuning the parameters, the procedure could be able to either fully mimic the surgeon or focus on obtaining viable and unconventional approaches, which might be used in surgical planning.

In terms of the path planning approach, it can be seen that typical approaches to path planning in surgical procedures often include Rapidly-exploring Random Trees (RRT) [5], [38], graph-based approaches (for instance: Dijkstra's algorithm) [30] or simple motion planners, usually based on user input or image processing [20], [21], [39]. However, the studies in which they are employed usually involve entire robotic systems for autonomous surgery or surgery planning and the test cases are based on simplified phantoms or computer generated environments, in which the collisive elements do not have a variable cost assigned to them. In this study, actual segmented images of the knee were employed and processed into cost maps. Furthermore, the results were compared to reference provided by a surgeon. To the best of our knowledge, such an approach was not undertaken before for medical path planning in knee surgery. On the other hand, the cases in this study did not account for tissue deformation, nevertheless, this problem is often solved by continuous path re-planning under magnetic resonance or ultrasound [38]. The proposed method could be also seen as a subset of reinforcement learning. With a wider database of reference paths, the procedure itself could be optimized to reproduce the output of an experienced surgeon. In such a case, the planned paths could be superimposed onto the image in head-mounted displays in augmented reality surgical systems [24].

5. Conclusions

In this paper, a procedure for automatic needle path planning in Baker's cyst aspiration was proposed and tested using 165 numerical simulations. In all of the 165 obtained paths, the needle successfully avoided crucial objects, such as nerves, veins and arteries. Furthermore, the overall travel distance in the joint was also minimized.

In general, the obtained results suggested a high correlation between the software and the approach of an experienced surgeon. Nevertheless, in some cases, the path generated by the procedure differed from the one proposed by the surgeon. In such cases, while both paths were technically feasible, the surgeon's path would be easier to execute during actual surgery. Based on the analysis of such cases, we believe that additional constraints should be imposed on the objective function to include the ease of executing the approach.

References

[1] ABATE M., DI CARLO L., DI IORIO A., SALINI V., *Baker's Cyst with Knee Osteoarthritis: Clinical and Therapeutic Implications*, Med. Princ. Pract., 2021, 30 (6), 585–591, DOI: 10.1159/000518792.

[2] ABU-DAKKA F.J., RUBIO F., VALERO F., MATA V., *Evolutionary indirect approach to solving trajectory planning problem for industrial robots operating in workspaces with obstacles*, Eur. J. Mech. – A/Solids, 2013, 42, 210–218, DOI: 10.1016/j.euromechsol.2013.05.007.

[3] AUBIN C.E., GOUSSEV V., PETIT Y., *Biomechanical modelling of segmental instrumentation for surgical correction of 3D spinal deformities using Euler-Bernoulli thin-beam elastic deformation equations*, Med. Biol. Eng. Comput., 2004, 42 (2), 216–221.

[4] BENNER R.W., SHELBOURNE K.D., BAUMAN S.N., NORRIS A., GRAY T., *Knee Osteoarthritis: Alternative Range of Motion Treatment*, Orthop. Clin. North Am., 2019, 50 (4), 425–432, DOI: 10.1016/j.ocl.2019.05.001.

[5] BERNARDES M.C., ADORNO B.V., POIGNET P., BORGES G.A., *Robot-assisted automatic insertion of steerable needles with closed-loop imaging feedback and intraoperative trajectory replanning*, Mechatronics, 2013, 23 (6), 630–645, DOI: 10.1016/j.mechatronics.2013.06.004.

[6] BLOME A., HARRIGAN R., GOETT H., COSTANTINO T., GIBBONS R., *Ultrasonographic Characteristics of Baker's Cysts: The Sonographic Foucher's Sign*, J. Emerg. Med., 2017, 53 (5), 753–755, DOI: 10.1016/j.jemermed.2017.08.029.

[7] CANOSO J.J., GOLDSMITH M.R., GERZOF S.G., WOHLGETHAN J.R., *Foucher's sign of the Baker's cyst*, Ann. Rheum. Dis., 1987, 46 (3), 228 LP – 232, DOI: 10.1136/ard.46.3.228.

[8] CHIRICHELLA P.S., JOW S., IACONO S., WEY H.E., MALANGA G.A., *Treatment of knee meniscus pathology: Rehabilitation, surgery, and orthobiologics*, PM R, 2019, 11 (3), 292–308, DOI: 10.1016/j.pmrj.2018.08.384.

[9] CISZKIEWICZ A., MILEWSKI G., *Comparison of methods for computing a target point for aspirations and biopsies*, [in:] *Biomechanics in Medicine and Biology*, K. Arkusz, R. Będziński, T. Klekiel, S. Piszczatowski (Eds.), BIOMECHANICS 2018. Advances in Intelligent Systems and Computing, Vol. 831. Springer, Cham, 2019, DOI: 10.1007/978-3-319-97286-2_8.

[10] CISZKIEWICZ A., MILEWSKI G., *Path planning for minimally-invasive knee surgery using a hybrid optimization procedure*, Comput. Methods Biomech. Biomed. Engin., 2018, 21 (1), 47–54, DOI: 10.1080/10255842.2017.1423289.

[11] CISZKIEWICZ A., MILEWSKI G., *Ligament-based spine-segment mechanisms*, Bull Polish Acad. Sci. Tech. Sci., 2018, 66 (5), 705–712, DOI: 10.24425/125337.

[12] DEMANGE M.K., *BAKER'S CYST*, Rev. Bras Ortop. (English Ed.), 2011, 46 (6), 630–633, DOI: 10.1016/S2255-4971(15)30317-7.

[13] DRAGAN S., KUROPKA P., KULEJ M., GABRYŚ P., NIKODEM A., *Changes in the mechanical properties of femoral cartilage tissue in advanced osteoarthritis*, Acta Bioeng. Biomech., 2020, 22 (1), 143–152, DOI: 10.37190/ABB-01463-2019-01.

[14] FERNER F., LUTTER C., SCHUBERT I., SCHENKE M., STRECKER W., DICKSCHAS J., *Perioperative complications in osteotomies around the knee: a study in 858 cases*, Arch. Orthop. Trauma Surg., 2022, 142 (5), 769–775, DOI: 10.1007/s00402-020-03696-w.

[15] FREDERICKSEN K., KIEL J., *Bedside ultrasound-guided aspiration and corticosteroid injection of a baker's cyst in a patient with osteoarthritis and recurrent knee pain*, J. Am. Coll. Emerg. Physicians Open, 2021, 2 (2), e12424, DOI: 10.1002/emp2.12424.

[16] GHADERI S., GHADERI K., GHAZNAVI H., *Using marker-controlled watershed transform to detect Baker's cyst in magnetic resonance imaging images: A pilot study*, J. Med. Signals Sensors, 2022, 12 (1), 84–89, DOI: 10.4103/jmss.JMSS_49_20.

[17] HASSOUNA M.S., FARAG A.A., HUSHEK S.G., *3D path planning for virtual endoscopy*, Int. Congr. Ser., 2005, 1281, 115–120, DOI: 10.1016/j.ics.2005.03.142.

[18] KORNAAT P.R., BLOEM J.L., CEULEMANS R.Y.T., RIYAZI N., ROSENDAAL F.R., NELISSEN R.G., CARTER W.O., HELLIO LE GRAVERAND M.-P., KLOPPENBURG M., *Osteoarthritis of the Knee: Association between Clinical Features and MR Imaging Findings*, Radiology, 2006, 239 (3), 811–817, DOI: 10.1148/radiol.2393050253.

[19] KRZEMIŃSKA K., CZAMARA A., *Diagnostic value of the hamstring to quadriceps ratio in monitoring the effectiveness of supervised 6-month physiotherapy in males after anterior cruciate ligament reconstruction (Aclr)*, Acta Bioeng. Biomech., 2020, 22 (4), 1–18, DOI: 10.37190/ABB-01656-2020-02.

[20] LIANG K., ROGERS A.J., LIGHT E.D., VON ALLMEN D., SMITH S.W., *Three-dimensional ultrasound guidance of autonomous robotic breast biopsy: feasibility study*, Ultrasound Med. Biol., 2010, 36 (1), 173–7, DOI: 10.1016/j.ultrasmedbio.2009.08.014.

[21] LIANG K., ROGERS A.J., LIGHT E.D., VON ALLMEN D., SMITH S.W., *Simulation of autonomous robotic multiple-core biopsy by 3D ultrasound guidance*, Ultrason Imaging, 2010, 32 (2), 118–127.

[22] LORKOWSKI J., KOLASZYŃSKA O., POKORSKI M., *Artificial Intelligence and Precision Medicine: A Perspective BT – Integrative Clinical Research*, in: M. Pokorski (ed.), Springer International Publishing, Cham., 2022, 1–11, DOI: 10.1007/5584_2021_652.

[23] MACIAZEK M., PASKO M., *Optimum allocation of active power filters in large supply systems*, Bull Polish Acad. Sci. Tech. Sci., 2016, 64 (1), 37–44, DOI: 10.1515/bpasts-2016-0005.

[24] MAJAK M., ŻUK M., ŚWIĄTEK-NAJWER E., POPEK M., PIETRUSKI P., *Augmented reality visualization for aiding biopsy procedure according to computer tomography based virtual plan*, Acta Bioeng. Biomech., 2021, 23 (2), 81–89, DOI: 10.37190/ABB-01811-2021-02.

[25] MARCHETTI C., BIANCHI A., MUYLDERMANS L., DI MARTINO M., LANCELLOTTI L., SARTI A., *Validation of new soft tissue software in orthognathic surgery planning*, Int. J. Oral Maxillofac. Surg., 2011, 40 (1), 26–32, DOI: 10.1016/j.ijom.2010.09.004.

[26] MICHAEL J.W.P., SCHLÜTER-BRUST K.U., EYSEL P., *Epidemiologie, ätiologie, diagnostik und therapie der gonarthrose*, Dtsch Arztebl., 2010, 107 (9), 152–162, DOI: 10.3238/arztebl.2010.0152.

[27] MORTADA M., AMER Y.A., ZAGHLOL R.S., *Efficacy and Safety of Musculoskeletal Ultrasound Guided Aspiration and Intra-Lesional Corticosteroids Injection of Ruptured Baker's Cyst: A Retrospective Observational Study*, Clin. Med. Insights Arthritis Musculoskelet. Disord., 2020, 13, 1179544120967383, DOI: 10.1177/1179544120967383.

[28] MOUSTRIS G.P., HIRIDIS S.C., DELIPARASCHOS K.M., KONSTANTINIDIS K.M., *Evolution of autnomous and semi-autnomous robotic surgical systems: a review of the literature*, Int. J. Med. Robot., 2011, 7 (April), 375–392, DOI: 10.1002/rcs.

[29] NAJMAEI N., MOSTAFAVI K., SHAHBAZI S., AZIZIAN M., *Image-guided techniques in renal and hepatic interventions*, Image-Guided Tech. Ren. Hepatic Interv., 2013, 9 (4), 379–395, DOI: 10.1002/rcs.

[30] NAPALKOVA L., ROZENBLIT J.W., HWANG G., HAMILTON A.J., SUANTAK L., *An optimal motion planning method for computer-assisted surgical training*, Appl. Soft Comput., 2014, 24, 889–899, DOI: 10.1016/j.asoc.2014.08.054.

[31] PARK G.-Y., KWON D.R., KWON D.G., *Clinical, Radiographic, and Ultrasound Findings Between Simple and Complicated Baker's Cysts*, Am. J. Phys. Med. Rehabil., 2020, 99 (1).

[32] PIETRUSKI P., MAJAK M., ŚWIĄTEK-NAJWER E., POPEK M., JAWOROWSKI J., ŻUK M., NOWAKOWSKI F., *Image-guided bone resection as a prospective alternative to cutting templates – A preliminary study*, J. Craniomaxillofac. Surg., 2015, 43 (7), 1021–7, DOI: 10.1016/j.jcms.2015.06.012.

[33] QURESHI A.H., AYAZ Y., *Intelligent bidirectional rapidly-exploring random trees for optimal motion planning in complex cluttered environments*, Rob. Auton. Syst., 2015, 68, 1–11, DOI: 10.1016/j.robot.2015.02.007.

[34] SILLAY K.A., RUSY D., BUYAN-DENT L., NINMAN N.L., VIGEN K.K., *Wide-bore 1.5 T MRI-guided deep brain stimulation surgery: initial experience and technique comparison*, Clin. Neurol. Neurosurg., 2014, 127, 79–85, DOI: 10.1016/j.clineuro.2014.09.017.

[35] STORN R., PRICE K., *Differential Evolution – A Simple and Efficient Heuristic for global Optimization over Continuous*

Spaces, J. Glob. Optim., 1997, 11 (4), 341–359, DOI: 10.1023/A:1008202821328.

[36] SU C., KUANG S., ZHAO X., LI Y., XIONG Y., GAO S., *Clinical outcome of arthroscopic internal drainage of popliteal cysts with or without cyst wall resection*, BMC Musculoskelet Disord., 2020, 21 (1), 440, DOI: 10.1186/s12891-020-03453-5.

[37] URŠIČ B., KOCJANČIČ B., ROMOLO A., IGLIČ A., KRALJ-IGLIČ V., ZUPANC O., *Assessment of coxarthritis risk with dimensionless biomechanical parameters*, Acta Bioeng. Biomech., 2021, 23 (1), 25–34, DOI: 10.37190/abb-01738-2020-03.

[38] VROOIJINK G.J., ABAYAZID M., PATIL S., ALTEROVITZ R., MISRA S., *Needle path planning and steering in a three-dimensional non-static environment using two-dimensional ultrasound images*, Int. J. Rob. Res., 2014, 33 (10), 1361–1374, DOI: 10.1177/0278364914526627.

[39] XU J., JIA Z., SONG Z., YANG X., CHEN K., LIANG P., *Three-dimensional ultrasound image-guided robotic system for accurate microwave coagulation of malignant liver tumours*, Int. J. Med. Robot Comput. Assist. Surg., 2010, 6 (June), 256–268.

[40] ZHANG M., LI H., WANG H., XI G., LI Y., ZHAO B., *Arthroscopic Internal Drainage with Cyst Wall Resection and Arthroscopic Internal Drainage with Cyst Wall Preservation to Treat Unicameral Popliteal Cysts: A Retrospective Case – Control Study*, Orthop. Surg., 2021, 13 (4), 1159–1169, DOI: https://doi.org/10.1111/os.12917.